Effect of Al_2O_3 on the Crystallization of Mold Flux for Casting High Al Steel

LEJUN ZHOU, WANLIN WANG, and KECHAO ZHOU

In order to lower the weight of automotive bodies for better fuel-efficiency and occupant safety, the demand for high Al-containing advanced high strength steel, such as transformation-induced plasticity and twinning-induced plasticity steel, is increasing. However, high aluminum content in steels would tend to significantly affect the properties of mold flux during the continuous casting process. In this paper, a kinetic study of the effect of Al_2O_3 content on the crystallization behavior of mold flux was conducted by using the single hot thermocouple technique and the Johnson–Mehl–Avrami model combined with the Arrhenius Equation. The results suggested that Al_2O_3 behaves as an amphoteric oxide in the crystallization process of mold flux. The precipitated phases of mold flux change from cuspidine ($Ca_4Si_2O_7F_2$) into nepheline ($NaAlSiO_4$) and CaF_2, and then into gehlenite ($Ca_2Al_2SiO_7$) with the increase of Al_2O_3 content. The kinetics study of the isothermal crystallization process indicated that the effective crystallization rate (k) and Avrami exponent (n) also first increased and then decreased with the increase of Al_2O_3 content. The values for the crystallization activation energy of mold flux with different Al_2O_3 contents were $E_{R0.8A7} = 150.76 \pm 17.89$ kJ/mol, $E_{R0.8A20} = 136.43 \pm 6.48$ kJ/mol, $E_{R0.8A30} = 108.63 \pm 12.25$ kJ/mol and $E_{R0.8A40} = 116.15 \pm 8.17$ kJ/mol.

DOI: 10.1007/s40553-015-0047-8

I. INTRODUCTION

IN order to lower the energy consumption, apart from developing advanced combustion systems to improve engine thermal efficiency, the applications of alternative lightweight materials to automotive construction will ensure higher fuel efficiency. Therefore, the development of lightweight automotive steel with high strength to improve fuel efficiency and occupant safety has attracted much attention. High Al steels, such as TRIP[1,2] (transformation-induced plasticity) steel with Al content of 0.5 to 2.0 pct and TWIP[3,4] (twinning-induced plasticity) steel, are the two important members of the family of high-strength automotive steels.

However, during the high Al steel continuous casting process, aluminum in the liquid steel tends to transfer into mold flux through two basic ways: absorption of alumina-based inclusions that formed during the processes of steelmaking, refining and continuous casting,[5,6] and the direct reaction between the Al in the molten steel and SiO_2 in the liquid mold flux layer at the steel–slag interface.[7,8]

According to the report from ArcelorMittal,[1] the pickup of Al_2O_3 content in the working mold flux can go higher than 30 pct during the continuous casting of high-aluminum transformation-induced plasticity (TRIP) steel. Kang *et al.*[9] investigated the reaction between high-alloyed twin-induced plasticity (TWIP) steel and molten mold flux through laboratory-scale experiments and kinetic analysis, and indicated that the Al_2O_3 pickup in the mold flux would be higher than 35 pct due to the slag/steel reaction.

The pickup of Al_2O_3 in the mold flux will lead to change of its properties, such as viscosity and crystallization, *etc.*, which then influences the process of continuous casting significantly. The influence of Al_2O_3 content on viscosity of the mold flux has been studied intensively.[10–15] All results suggested that the viscosity of the mold flux increased dramatically with the increase of Al_2O_3 content. However, the effect of Al_2O_3 content on the crystallization of mold flux has been conducted relatively less compared with viscosity from previous published literatures. Wang *et al.*[16] studied the crystallization behavior of a CaO-SiO_2-based mold flux used in the casting of transformation-induced plasticity steels, and the results indicated that the addition of alumina in the mold flux caused the transformation of crystallized phase, and the precipitation of CaF_2 was found in high temperature zone. Zhang *et al.*[17] investigated the influence of the mass ratio of Al_2O_3/SiO_2 on the crystallization behavior of mold flux, and found that the crystallization temperature increased due to the precipitation of CaF_2. Ryu *et al.*[18] reported that the crystallization temperature increased while the incubation time decreased with the increase of Al_2O_3 content ranging from 3.5 to

LEJUN ZHOU, Post Doctor, is with the School of Metallurgy and Environment, Central South University, Changsha 410083, P.R. China, and also with the State Key Laboratory of Power Metallurgy, Central South University, Changsha 410083, P.R. China. WANLIN WANG, Shenghua Professor, is with the School of Metallurgy and Environment, Central South University. Contact e-mail: wanlin.wang@gmail.com KECHAO ZHOU, Professor, is with the State Key Laboratory of Power Metallurgy, Central South University.

Manuscript submitted January 6, 2015.
Article published online March 27, 2015

25.39 wt pct, and the crystalline phase changed from $Ca_4Si_2O_7F_2$ to $Ca_2Al_2SiO_7$.

Although some research has been carried out, it still necessary to systematically study the effect of Al_2O_3 content on the crystallization behavior of mold flux, due to the importance of the crystallization of mold flux on the shell lubrication and heat transfer in the mold.[19,20] Therefore, in this paper, a kinetic study of the effect of Al_2O_3 content on the crystallization behavior of mold flux will be conducted. The continuous cooling transformation (CCT) and temperature time transformation (TTT) diagrams of low basicity mold flux with Al_2O_3 content ranging from 7 to 40 wt pct will be constructed by using single hot thermocouple technology (SHTT); and the precipitated phase will be detected by X-ray diffraction (XRD). Also, the isothermal crystallization behavior of mold flux will be analyzed by using a kinetic method combining the Johnson–Mehl–Avrami (JMA) model and the Arrhenius Equation.

II. EXPERIMENTAL METHOD

A. *Design of Experimental Slags*

The matrix flux (named R0.8A7 in Table I) used in this study is an industrial low carbon steel mold flux with the basicity (R = CaO/SiO_2) of 0.8 and Al_2O_3 content of 7 wt pct, and its crystallization ability is rather low as shown in a previous paper.[21] In order to study the effect of Al_2O_3 on the crystallization behavior of mold flux, different amounts of reagent grade chemicals of CaO, Al_2O_3, MgO, CaF_2, Na_2O and Li_2O were added to the R0.8A7 mold flux to adjust the Al_2O_3 content, changing it from 7 to 40 pct, meanwhile keeping other components balanced. The maximal amount of Al_2O_3 was chosen as 40 pct according to the CaO-SiO_2-Al_2O_3 ternary phase diagram,[22] in which the maximal amount of Al_2O_3 in the precipitation zone for Corundum is about 40 pct when the CaO/SiO_2 = 0.8 (see Figure 1). The mixtures were melted in an induction furnace at 1773 K (1500 °C) for 5 minutes to homogenize its chemical composition. Then, it was poured onto a cool steel plate to quench, and then subjected to crushing and grinding to make sample powders for the SHTT measurements. The final pre-melted slags were analyzed by X-ray fluoroscopy (XRF), and their chemical compositions are marked as dots in Figure 1 and listed in Table I.

B. *CCT Test*

The CCT tests of the mold flux were conducted by using SHTT, while the details of SHTT/DHTT have been described by Kashiwaya *et al.*,[23] as shown in Figure 2.

When conducting the CCT tests, the thermocouple together with the powder sample was first heated to 1773 K (1500 °C) with a rate of 15 K (°C)/s; then it was held for 180 seconds to eliminate bubbles and homogenize its chemical composition. Next, it was cooled with a certain cooling rate. The phase transformation from molten to crystalline or glass could be observed and recorded through the attached CCD. Meanwhile, the temperature of sample was also collected and saved by the temperature acquisition system. Figure 3 is the schematic of the temperature controlling profile for the CCT test. The CCT diagrams of the mold flux were

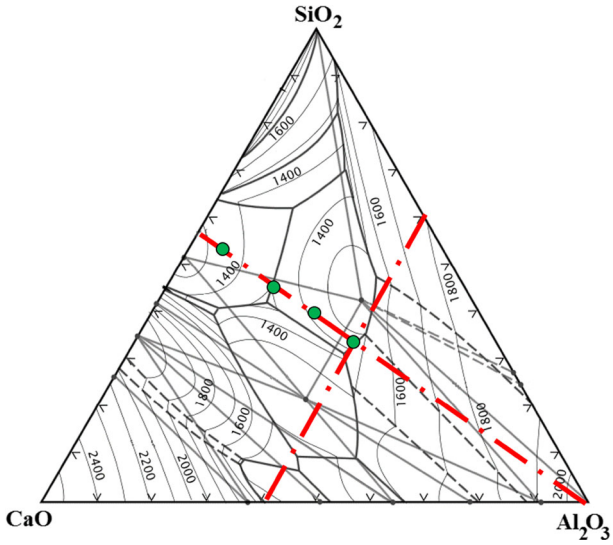

Fig. 1—CaO-SiO_2-Al_2O_3 ternary phase diagram[19].

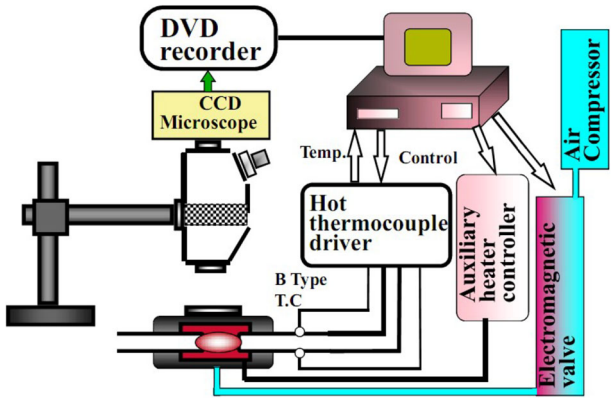

Fig. 2—Schematic of the experimental apparatus.[20]

Table I. The Chemical Compositions of Mold Fluxes with Different Al_2O_3 Content After Pre-melted (in Weight Percent)

	CaO	SiO_2	Al_2O_3	MgO	F	Na_2O	Li_2O	R
R0.8A7	33.53	42.05	7.02	2.00	5.88	9.02	0.50	0.8
R0.8A20	27.84	34.70	20.01	2.02	5.91	9.02	0.50	0.8
R0.8A30	23.37	29.16	30.01	2.01	5.94	9.01	0.50	0.8
R0.8A40	18.89	23.60	40.00	2.00	5.98	9.01	0.50	0.8

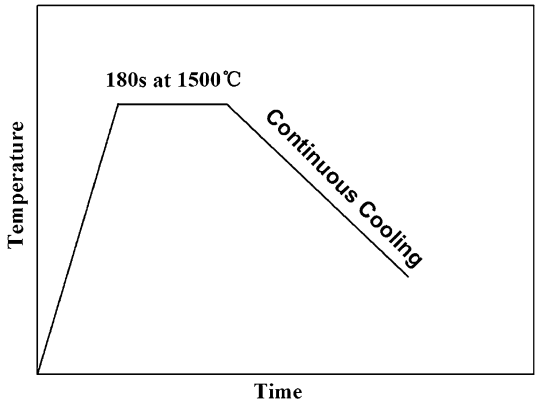

Fig. 3—Schematic of temperature profile during the CCT tests.

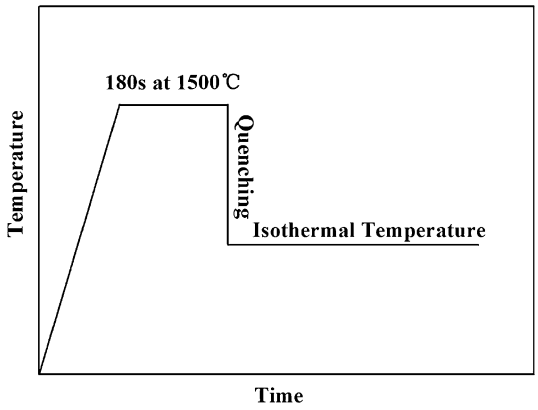

Fig. 4—Schematic of temperature control during the TTT tests.

constructed by the corresponding relationships between the temperature, time, and phase fraction.

C. *TTT Test*

The TTT tests were also carried out by using the SHTT, and its temperature controlling profile is schematically shown in Figure 4. For the TTT test, the sample was first heated to 1773 K (1500 °C) with the rate of 15 °C/s and held for 180 seconds. Next, unlike the CCT tests, the sample was cooled rapidly to different temperatures and held for isothermal crystallization. The TTT diagrams of mold flux were also constructed through the corresponding relationships between the temperature, time, and phase fraction during the TTT test process.

D. *Kinetic Analysis Method*

The kinetics of mold flux isothermal crystallization involving nucleation and growth was analyzed through the JMA model,[24,25] according to which the volume fraction of crystals (X) was given by:

$$X = 1 - \exp\{-[k(t-\tau)]^n\} \qquad [1]$$

where t is crystallization time, τ is incubation time, k is the effective crystallization rate constant (including nucleation and growth), and n is the Avrami exponent.

The volume fraction of crystallization (X) obtained at a certain temperature was defined as $X = A_c/A_T$, where A_C is the area of crystal and A_T is the total area of the mold flux. The values of A_C and A_T were obtained by image analysis. Figure 5 shows a schematic of variation of the crystal volume fraction.

Therefore, the values of n and k could be determined according to the following equation by rearranging Eq. [1] into Eq. [2]

$$\ln\ln\left(\frac{1}{1-X}\right) = n\ln k + n\ln(t-\tau) \qquad [2]$$

By plotting $\ln\ln(1-X)$ *vs* $\ln(t-\tau)$, the values of k and n could be obtained as the interception and slope of the regression line, respectively.

The effective crystallization rate constant (k) that was related to temperature T could also be determined via the Arrhenius Equation:[26,27]

$$k = A\exp\left(\frac{-E_a}{RT}\right) \qquad [3]$$

where, E_a is the activation energy of crystallization, A stands for the pre-exponential factor, R is the gas constant, and T the absolute temperature (note the unit is K).

By rearranging Eq. [3], the value of E_a could also be determined by plotting $\ln k$ *vs* $1/(RT)$ from Eq. [4].

$$\ln k = \ln A - \frac{E_a}{RT} \qquad [4]$$

Therefore, the effect of Al_2O_3 on mold flux crystallization could be analyzed through the above kinetic study.

E. *Phases Identification Method*

X-ray diffraction was used to identify the precipitated phases of the mold flux under different temperatures. Because the amounts of the samples of the SHTT tests are too small for X-ray diffraction (XRD) analysis, the samples for XRD were prepared in a $MoSi_2$ furnace. First, the $MoSi_2$ furnace with 30 g of well-mixed mold flux powders was heated to 1573 K (1300 °C); and then the mold flux was melted and homogenized for 180 seconds. Next, the furnace was cooled to the target temperature with a cooling rate of 5 K (°C)/s, and then held 10 hours for isothermal crystallization. Finally, the mold flux was cooled to room temperature, then crushed and ground into powder samples for XRD analysis. The XRD data were collected by using Cu Kα radiation (1.54184 Å), in a range of 2θ = 10 to 80 deg with a step size of 2 deg/s.

III. RESULTS AND DISCUSSION

A. *The Effect of Al_2O_3 Content on Continuous Cooling Crystallization Behavior of Mold Flux*

The CCT diagrams of four series of mold fluxes are shown in Figure 6, with mold fluxes with Al_2O_3 content

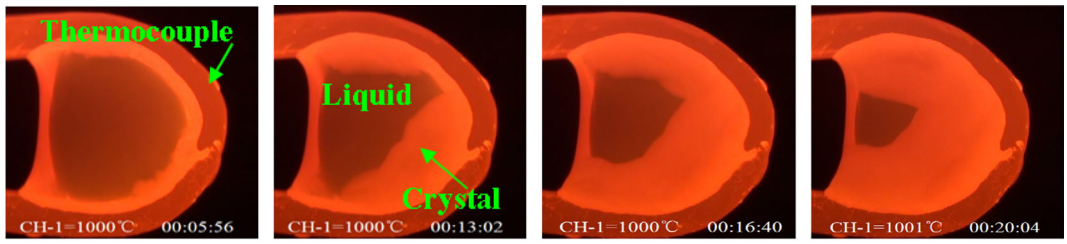

Fig. 5—Schematic of variation of volume fraction of crystallites.

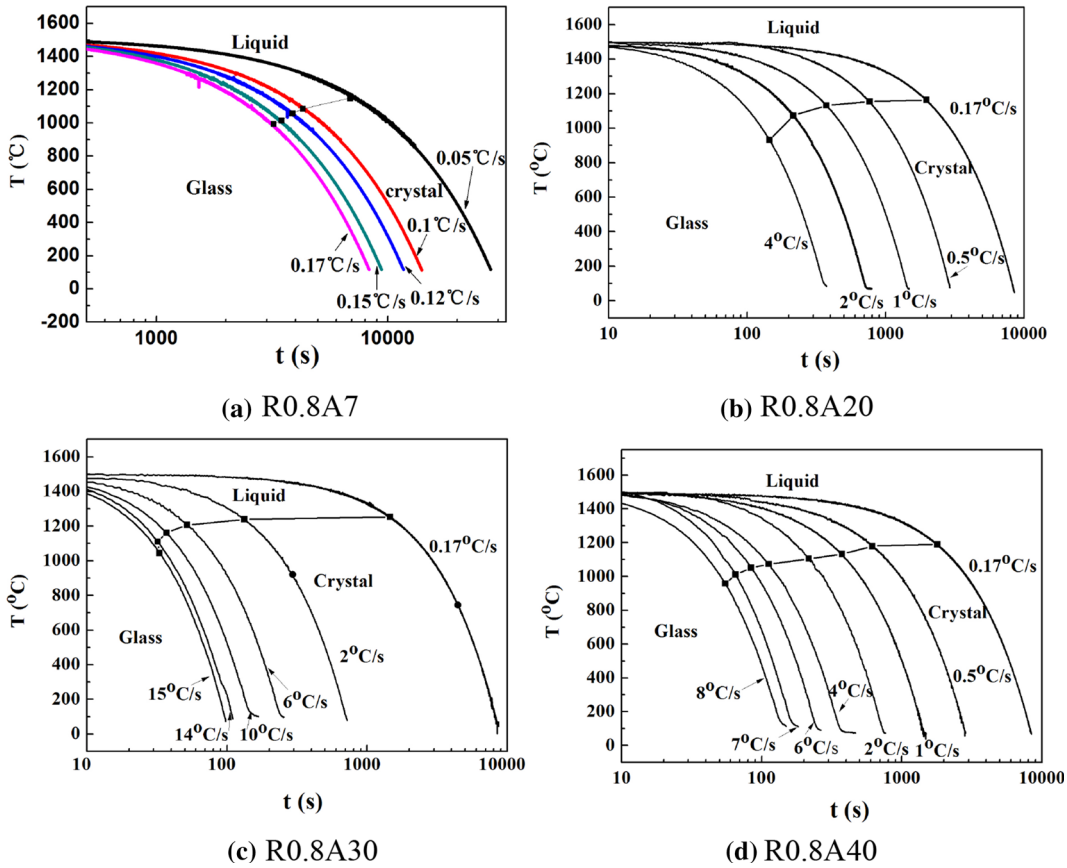

Fig. 6—CCT diagrams of mold fluxes with different Al_2O_3 contents.

of 7, 20, 30 and 40 pct, respectively. It can be seen from Figure 6 that there are three phase zones in CCT diagram, which are the high-temperature liquid phase and the low-temperature glassy or crystalline phases. Typically, there is a key parameter, the critical cooling rate, which will determine whether the mold flux will transform into the glassy or crystalline phase. For example, the CCT diagram of mold flux R0.8A7 (Figure 6(a)) indicates that the crystal will precipitate in the molten slag when the cooling rate is lower than 0.17 °C/s; otherwise, glass will be formed when the cooling rate is higher than 0.17 °C/s. Therefore, the 0.17 °C/s is the critical cooling rate of mold flux R0.8A7. In addirion, it can also be seen from Figure 6 that the initial crystallization temperature decreases with the increase of cooling rate, which results from the increase of molten slag viscosity with the addition of the cooling rate, which requires a larger driving force to initiate the crystallization during the continuous cooling process of the mold flux.[21]

In order to further study the effect of Al_2O_3 content on the critical cooling rate and crystallization temperature of mold fluxes, the critical cooling rates and the crystallization temperatures under the cooling rate of 0.17 °C/s are shown in Figures 7 and 8, respectively. Figure 7 suggests that the critical cooling rate of mold flux first increases and then decreases with the addition of Al_2O_3 content. The values for critical cooling rate are 0.17, 4, 15 and 8 °C/s when the corresponding mold fluxes contain Al_2O_3 of 7, 20, 30 and 40 pct, respectively. This kind of trend can also be seen from Figure 8 where the crystallization temperature of mold fluxes first

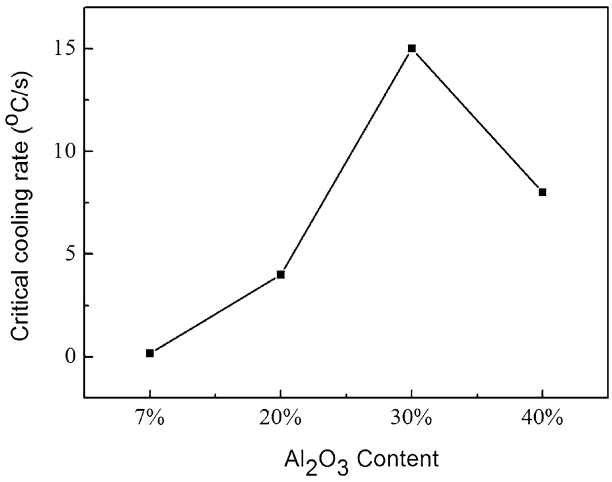

Fig. 7—The critical cooling rates of mold fluxes with different Al_2O_3 contents.

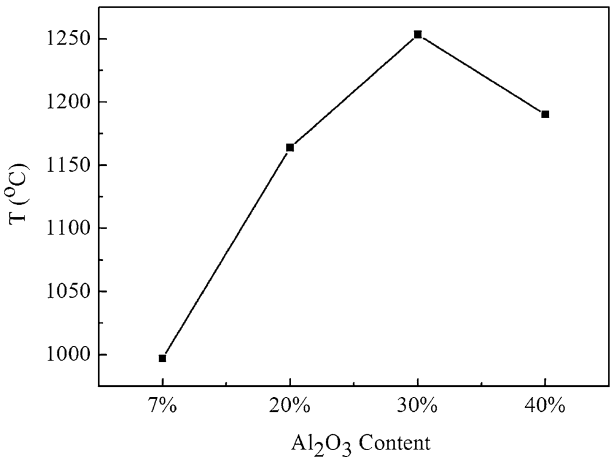

Fig. 8—The crystallization temperature of mold fluxes with different Al_2O_3 contents under cooling rate of 0.17 °C/s.

increases and then decreases. When the Al_2O_3 content is 7 pct, the crystallization temperature is 1270 K (997 °C), which will increase to 1526 K (1253 °C) when the Al_2O_3 content is 30 pct, then decrease to 1463 K (1190 °C) with the Al_2O_3 content changes from 30 to 40 pct.

The variance trend of the influence of Al_2O_3 content on both the critical cooling rate and crystallization temperature of the mold flux indicates that the Al_2O_3 has an amphoteric effect on the continuous cooling crystallization behavior of the mold flux. In fact, the Al_2O_3 is a typical amphoteric oxide,[28,29] and the amphoteric mechanism of Al_2O_3 in molten slag is schematically shown in Figure 9. When Al_2O_3 is added to acidic slag, it will work as a basic oxide to offer the O^{2-} and break the Si-O-Si bond, then increase the amount of non-bridging oxygen in the molten slag, consequently simplifying the silicate structure. The Al element will enter into the interstices of the silicate structure in the state of the Al^{3+} ions, as shown in Figure 9(a). In contrast, when Al_2O_3 is added to basic

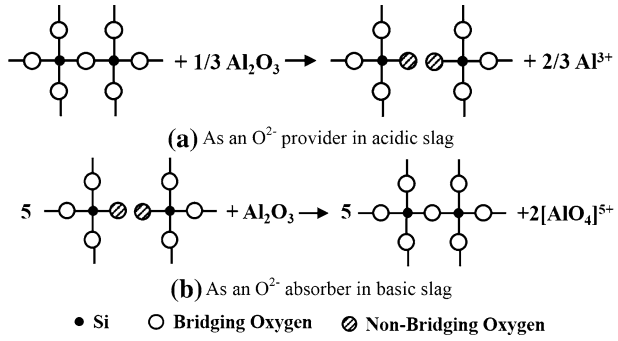

Fig. 9—The amphoteric mechanism of Al_2O_3 in molten slag.

slag, it will work as an acidic oxide that will absorb the O^{2-} and decrease the non-bridging oxygen in the molten slag, resulting in a higher polymerization degree of the silicate. The Al element will form the $[AlO_4]^{5+}$ unit just like $[SiO_4]^{4+}$ tetrahedral units, as shown in Figure 9(b). The basicity of matrix flux R0.8A7 is 0.8, which means it belongs to acidic slag. Thus, the added Al_2O_3 acted as a basic oxide to simplify the silicate structure and lower the viscosity of the molten slag, which is beneficial for the continuous cooling crystallization of the mold flux. However, the function of Al_2O_3 transferred from basic oxide to acidic oxide with the continuous increase of Al_2O_3 from 30 to 40 pct as the matrix flux itself changed to basic, and the silicate network changed into a more complex alumino-silicate structure.[30] Thus, the crystallization ability of the mold flux in the continuous cooling process was getting weaker when the Al_2O_3 content was about 40 pct, compared to when the Al_2O_3 content was 30 pct.

B. *The Effect of Al_2O_3 Content on the Isothermal Crystallization Behavior of Mold Flux*

Figure 10 shows the TTT diagrams of the above four series of mold fluxes. In this study, the crystalline fraction of 0.5 was defined as the beginning of crystallization, and crystalline fraction of 0.95 was defined as the end of crystallization. It can be seen from Figure 10 that the TTT curve of mold flux R0.8A7 is the only one with a single "C" type shape; while the other three mold fluxes show a double "C" shape. The double "C" TTT curves indicate that the main precipitated phases in the high-temperature zone and the low-temperature zone are different, while the single "C" means there only one main phase existed when the mold flux became crystallized. In order to identify the phase compositions of crystals at the different temperature zones of the TTT diagram, the mold fluxes at certain temperatures were analyzed by using XRD, and the cooling curves for the preparation of XRD samples are shown in Figure 10.

The XRD results are shown in Figure 11. It was found that the precipitated phase of mold flux R0.8A7 is cuspidine ($Ca_4Si_2O_7F_2$), which is quite common in mold fluxes. When the Al_2O_3 content in mold flux R0.8A20 was increased to 20 pct, the nepheline ($NaAlSiO_4$) appeared in addition to $Ca_4Si_2O_7F_2$. It should be noticed that the $NaAlSiO_4$ not only formed in the low-

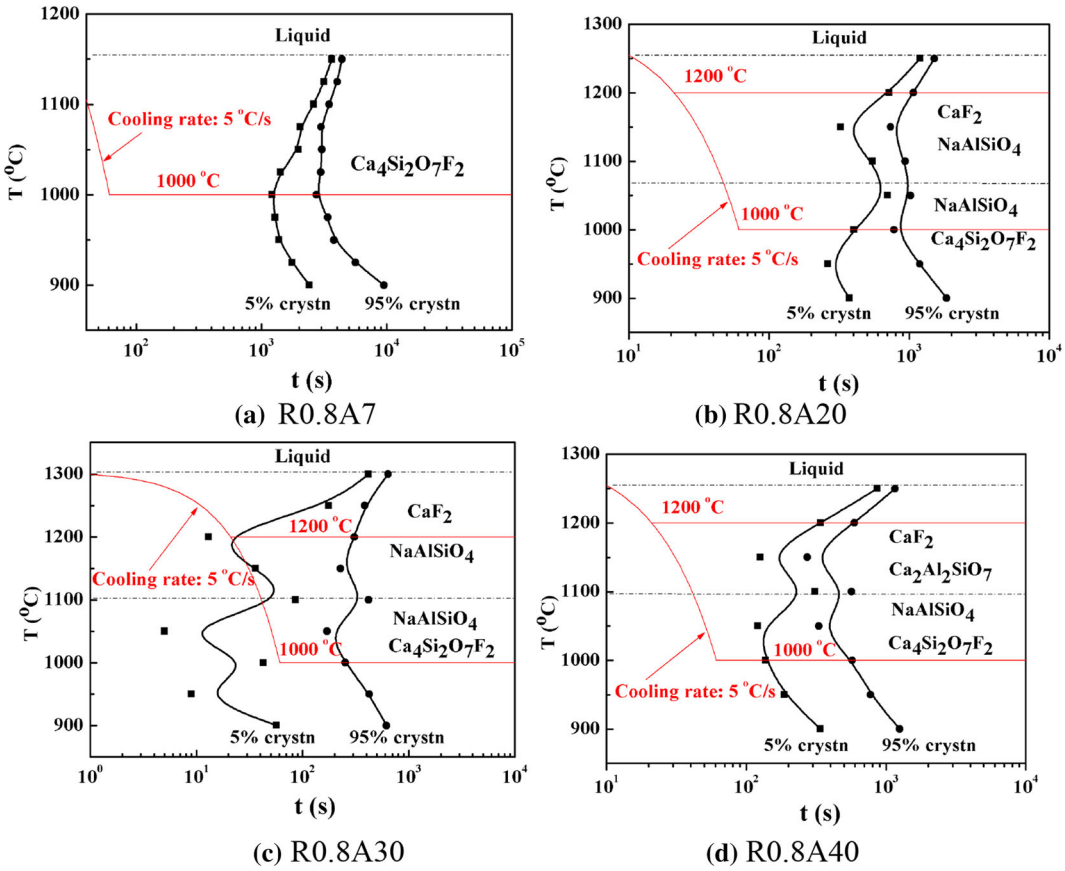

Fig. 10—The TTT diagrams of mold fluxes with different Al_2O_3 contents.

temperature zone but also in the high-temperature zone; and some CaF_2 was also detected in the high-temperature zone which is consistent with the result of Wang's research.[16] When the Al_2O_3 content reached 30 pct (mold flux R0.8A30), although the phase compositions of crystals in both the low- and high-temperature zones are similar to mold flux R0.8A20, the amount of CaF_2 increased, as the characteristic peak of CaF_2 in Figure 11(c) is higher than in Figure 11(b), which suggests that the Al_2O_3 can enhance the precipitation of the CaF_2 crystals. Finally, when the Al_2O_3 content was further increased to 40 pct (mold flux R0.8A40), the crystal phase precipitated in the high-temperature zone changed into gehlenite ($Ca_2Al_2SiO_7$) as shown in Figure 11(d).

There are two basic reasons for the precipitation of $NaAlSiO_4$: (1) with the increase of Al_2O_3 content, silica tends to react with Al and Na to form $NaAlSiO_4$, as the trivalent Al^{3+} plus the univalent Na^+ can make the electrical charge balance with $[SiO_4]^{4-}$, hence the $NaAlSiO_4$ crystal forms; and (2) the precipitation temperature of $NaAlSiO_4$ crystal ranges from 1005 K to 1553 K (732 °C to 1280 °C) from the Na_2O-Al_2O_3-SiO_2 ternary phase diagram (see Figure 12),[22] so the $NaAlSiO_4$ may also form in both the high- and low-temperature zones in TTT diagrams (Figures 10(b) through (d)).

For the precipitation of CaF_2 in the high-temperature zone, it occurs because the crystallization temperature of CaF_2 itself is very high, about 1675 K (1402 °C). However, for the precipitation phase of $Ca_2Al_2SiO_7$ in the high-temperature zone of the TTT diagram of mold flux R0.8A40, this occurs because the Al behaves as an acidic oxide to form the $[AlO_4]^{5-}$ tetrahedral structures which are similar to Si, as the matrix flux itself changed to basic when the Al_2O_3 content is 40 pct; therefore, there are enough vacancy spaces for larger cations like Ca^{2+} to accede into the tetrahedral structures to form $Ca_2Al_2SiO_7$. In addition, the melting (or crystallization) temperature of $Ca_2Al_2SiO_7$ is higher than $NaAlSiO_4$,[22] thus the $Ca_2Al_2SiO_7$ can precipitate in the high-temperature zone of the TTT diagram of mold flux R0.8A40.

The incubation time is an important parameter to characterize the isothermal crystallization behavior of mold fluxes, just like the critical cooling rate is to the continuous cooling crystallization process. A shorter incubation time suggests an easier isothermal crystallization process. In order to investigate the influence of Al_2O_3 on the isothermal crystallization of the mold flux, the initial crystallization TTT curves of the four series os mold fluxes were combined and are shown in Figure 13. Also, the incubation times of mold fluxes with different Al_2O_3 contents at 1273 K (1000 °C) are given in Figure 14. From both Figures 13 and 14, it can be seen that the incubation time of isothermal crystallization first decreases and then increases with the further addition of Al_2O_3 content. For example, the incubation time reduces from 1213 to 43 seconds when the Al_2O_3

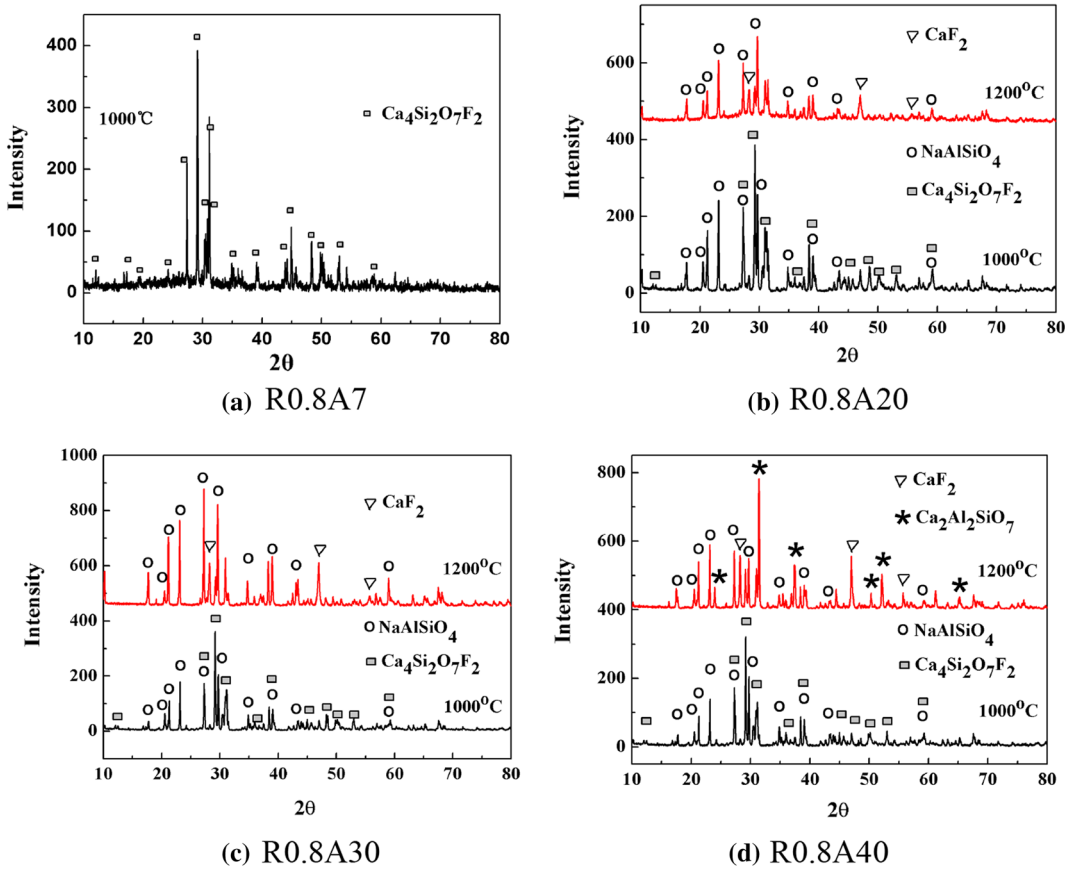

Fig. 11—The XRD of mold fluxes with different Al_2O_3 contents.

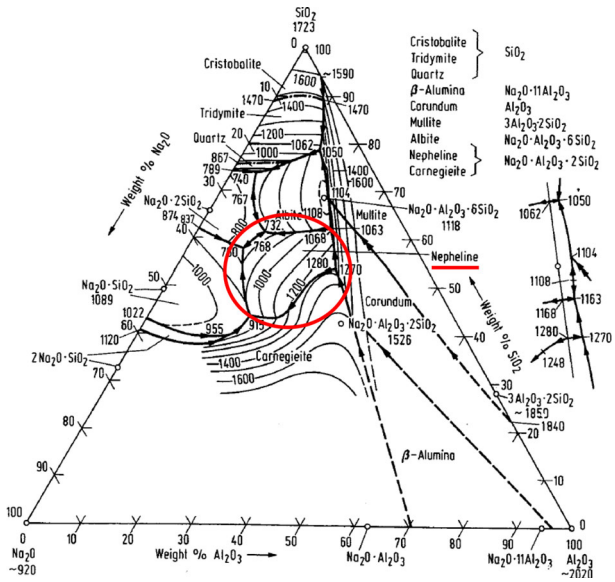

Fig. 12—Na_2O-Al_2O_3-SiO_2 ternary diagram.[19]

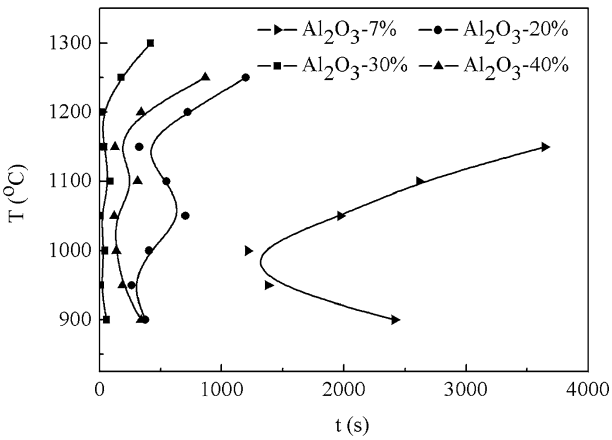

Fig. 13—Five pct of crystallization of mold flux with different Al_2O_3 contents.

content increases from 7 to 30 pct, while it gradually increases to 138 seconds with the Al_2O_3 increase to 40 pct, when the mold flux crystallizes at the temperature of 1273 K (1000 °C). The variation of incubation time with Al_2O_3 content suggests that the Al_2O_3 will enhance the isothermal crystallization of mold fluxes within a certain range of quantity, while it will behave in the opposite direction when its content exceeds that quantity. This kind of trend is consistent with the result of the continuous cooling crystallization process of mold fluxes as analyzed in Section III–A.

C. *The Kinetic Analysis of Mold Flux Crystallization*

Because the precipitated phases in the lower part of the TTT diagrams are similar, the isothermal crystallization processes at temperatures ranging 1173 K to 1323 K (900 °C to 1050 °C) were chosen as representative for the kinetic study. Plots of $\ln(\ln(1/1 - X))$ *vs* $\ln(t - \tau)$ for each individual mold flux crystallization are shown in Figures 15(a) through (d). The Avrami exponent n and the effective crystallization rate k are obtained as the slope of the regression line and the interception, respectively, as shown in Eq. [3]. The values of n and k are listed in Table II.

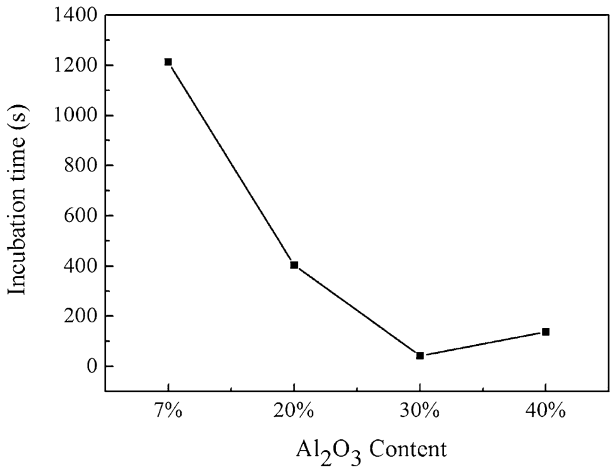

Fig. 14—Incubation times of mold fluxes with different Al_2O_3 contents at 1273 K (1000 °C).

The variations of k and n in Table II suggest that the effective crystallization rate and the Avrami exponent are functions of both temperature and Al_2O_3 content in mold fluxes. First, the values of k increase with the increase of holding temperature for each individual mold flux, which indicates that the mold flux can become crystallized more quickly with the increase of temperature, in the range of 1173 K to 1323 K (900 °C to 1050 °C). The reason for that is that the polymerization of silicate structures can be broken more easily under a higher temperature environment, which will lower the viscosity of the molten slag that is beneficial for the ions transfer and crystallization process. Secondly, the values of k first increase and then later decrease with the further addition of Al_2O_3 content, which is due to the amphoteric behavior of Al_2O_3 as shown in Figure 9.

According to the JMA isothermal crystallization theory, different Avrami exponents, n, stand for differ-

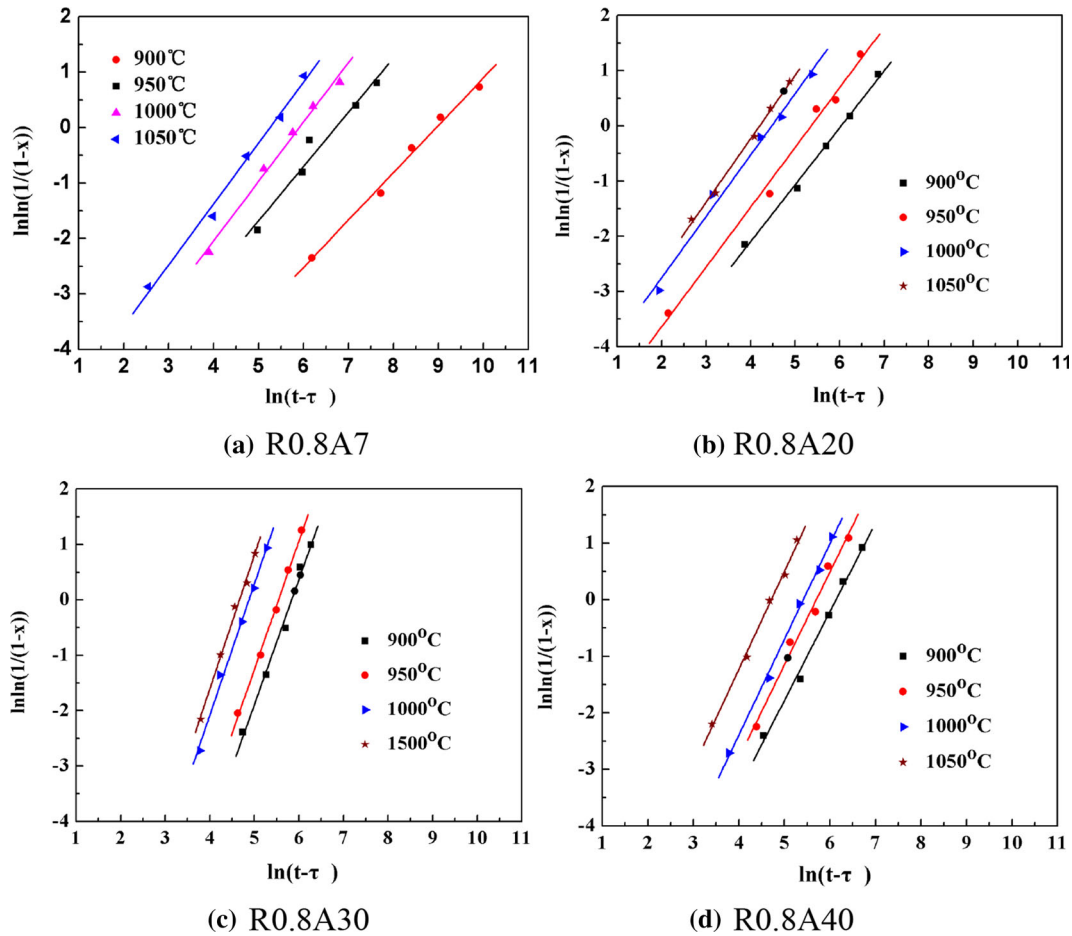

Fig. 15—The relation of crystalline volume fraction evolution with function of time.

Table II. The Variations of n and ln k as the Al_2O_3 Content and Temperature Changed

Al_2O_3 (in Mass Percent)	Temperature [K (°C)]	n	ln k
7	1173 K (900 °C)	0.85	−7.59
	1223 K (950 °C)	0.98	−6.67
	1273 K (1000 °C)	1.07	−6.31
	1323 K (1050 °C)	1.10	−5.77
20	1173 K (900 °C)	1.03	−6.25
	1223 K (950 °C)	1.08	−5.82
	1273 K (1000 °C)	1.11	−4.91
	1323 K (1050 °C)	1.15	−4.80
30	1173 K (900 °C)	2.26	−5.84
	1223 K (950 °C)	2.31	−5.55
	1273 K (1000 °C)	2.37	−4.88
	1323 K (1050 °C)	2.42	−4.66
40	1173 K (900 °C)	1.57	−6.12
	1223 K (950 °C)	1.64	−5.70
	1273 K (1000 °C)	1.69	−5.42
	1323 K (1050 °C)	1.73	−4.71

ent crystallization mechanisms. The relationship between n and the crystallization mechanism has been well described by Christian[31] and other researchers.[31–33] It can be found that the growth mechanism of the crystalline phase in the mold fluxes with Al_2O_3 content of 7 and 20 pct is 1-D (dimensional) growth with a constant number of nuclei as their n values approximate to 1. The growth mechanism of the mold flux crystalline phase changed to combined 2-D and 3-D when the corresponding Al_2O_3 content was 30 pct as its n value is close to 2.5. It changes to combined 1-D and 2-D growth when the addition of Al_2O_3 content was 40 pct, as its average n values at different temperatures are around 1.66. The above variation of n values with the addition of Al_2O_3 content suggests that Al_2O_3 has a big impact on the crystallization mechanism of the mold flux.

Figure 16 shows the plots of ln k *vs* $1/RT$ for the four series of mold fluxes with Al_2O_3 contents of 7, 20, 30 and 40 pct. The crystallization activation energy (E_a) was calculated from the slopes of linear fits to the experimental data as expressed in Eq. [4]. The results suggest that the crystallization activation energies are $E_{R0.8A7} = 150.76 \pm 17.89$ kJ/mol, $E_{R0.8A20} = 136.43 \pm 6.48$ kJ/mol, $E_{R0.8A30} = 108.63 \pm 12.25$ kJ/mol and $E_{R0.8A40} = 116.15 \pm 8.17$ kJ/mol for the four series, which indicate that the crystallization activation energy first decrease and then increase with the increase of Al_2O_3 content. The reason for that may also be associated mainly with the amphoteric effect of Al_2O_3 on the silicate structure of mold fluxes as discussed above. When the Al_2O_3 worked as basic oxide, it would simplify the silicate structure and decrease the viscosity of mold flux, which would reduce the transfer resistance of ion clusters and decrease the energy barrier for the nucleation and growth of crystals. In contrast, when the addiitional Al_2O_3 is in excess, it would increase the polymerization degree of the silicate, and then increase the energy barrier of the mold flux for nucleation and growth.

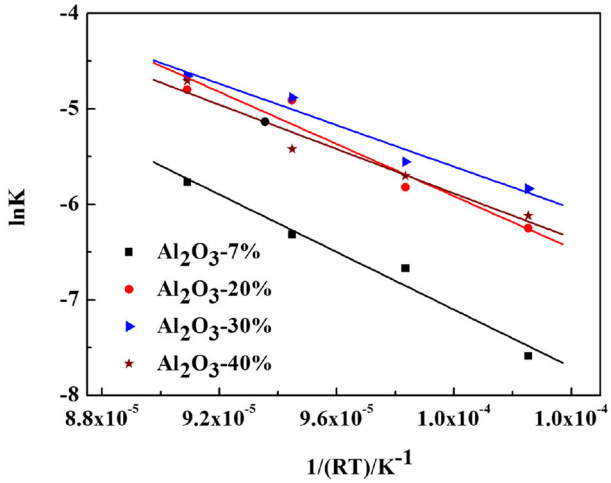

Fig. 16—Plots of ln k *vs* $1/RT$ for mold fluxes with different Al_2O_3 contents.

IV. CONCLUSIONS

With the aim of accelerating the industry-scale production of high Al-containing advanced high strength steel, such as TRIP and TWIP steel, a kinetic study of the effect of Al_2O_3 on the crystallization behavior of continuous casting mold flux was conducted by using the single hot thermocouple technique and the JMA model combined with the Arrhenius equation. The main conclusions can be summarized as follows:

1. The results of continuous cooling crystallization of mold flux show that the values of the critical cooling rate of the mold flux increase from 0.17, to 4 °C/s, and then to 15 °C/s when the Al_2O_3 content increases from 7, to 20 pct, and then to 30 pct, while it decreases to 8 °C/s when the Al_2O_3 content continuously increases to 40 pct. This kind of trend is similar to the crystallization temperatures of mold fluxes under the cooling rate of 0.17 °C/s, which are 1270 K, 1436 K, 1526 K, and 1463 K (997 °C, 1163 °C, 1253 °C, and 1190 °C) when the Al_2O_3 content is 7, 20, 30, and 40 pct, respectively.
2. The investigation of the isothermal crystallization behavior of the mold flux suggests that only the TTT curves of mold flux R0.8A7 is single "C" type, while the other three mold fluxes are obviously of the double "C" type. The incubation time first reduces and then increases with the increase of Al_2O_3 content. In addition, the precipitated phases of the mold fluxes change from cuspidine ($Ca_4Si_2O_7F_2$) into nepheline ($NaAlSiO_4$) and CaF_2, then into gehlenite ($Ca_2Al_2SiO_7$) with the increase of Al_2O_3 content.
3. The kinetics study of isothermal crystallization process indicated that the effective crystallization rate constant k and Avrami exponent n first increase and then later decrease with the Al_2O_3 content increase. The crystallization activation energy of the mold fluxes with different Al_2O_3 contents are

$E_{R0.8A7} = 150.76 \pm 17.89$ kJ/mol, $E_{R0.8A20} = 136.43 \pm 6.48$ kJ/mol, $E_{R0.8A30} = 108.63 \pm 12.25$ kJ/mol and $E_{R0.8A40} = 116.15 \pm 8.17$ kJ/mol.

4. The different influence trends between lower and higher Al_2O_3 contents on continuous cooling crystallization and isothermal crystallization behavior of mold fluxes basically result from the amphoteric behavior of Al_2O_3. When the Al_2O_3 content is less than 30 pct, it will work as a silicate network modifier and enhance the crystallization, while it will work as network former and inhabit the crystallization when Al_2O_3 content of the mold fluxes used in this study increases from 30 to 40 pct.

ACKNOWLEDGMENTS

The authors wish to thank the China Postdoctoral Science Foundation (2014M550423), and The Hunan Provincial Science and Technology Program (2014TT 2030) for support of this research.

REFERENCES

1. K. Blazek, H. Yin, G. Skoczylas, M. McClymonds, and M. Frazee: *Iron Steel Technol*., 2011, vol. 8, pp. 232–40.
2. J.G. Speer, E.D. Moor, and K. Matlock: BAC, Shanghai, China, 2010, p. E-1.
3. L. Chen, Y. Zhao, and X. Qin: *Acta Metall. Sin*., 2013, vol. 26, pp. 1–15.
4. S. Hong, S.Y. Shin, H.S. Kim, S. Lee, S. Kim, K. Chin, and N.J. Kim: *Metall. Mater. Trans. A*, 2012, vol. 43A, pp. 1870–83.
5. L. Zhang and B.G. Thomas: *XXIV National Steelmaking Symposium*, Morelia, Mich, Mexico, 26–28, 2003, pp. 457–520.
6. H.V. Atkinson and G. Shi: *Prog. Mater. Sci*., 2003, vol. 48, p. 457.
7. J. Park, S. Seetharaman, and R.J. Fruehan: *Iron Steel Technol*., 2012, vol. 9, pp. 86–93.
8. M. Kim, S. Lee, J. Cho, M. Park, H. Lee, and Y. Kang: *Metall. Mater. Trans. B*, 2013, vol. 44B, pp. 299–308.
9. Y. Kang, M. Kim, S. Lee, J. Cho, M. Park, and H. Lee: *Metall. Mater. Trans. B*, 2013, vol. 44B, pp. 309–16.
10. K.C. Mills, A.B. Fox, Z. Li, and R.P. Thackray: *Ironmak. Steelmak*., 2005, vol. 32, pp. 26–34.
11. Z. Zhang, G. Wen, P. Tang, and S. Sridhar: *ISIJ Int*., 2008, vol. 48, pp. 739–46.
12. G. Kim and I. Sohn: *J. Non-Cryst. Solids*, 2012, vol. 358, pp. 1530–37.
13. X. Yu, G.H. Wen, P. Tang, and H. Wang: *Ironmak. Steelmak*., 2009, vol. 36, pp. 623–30.
14. F. Shahbazian, D. Sichen, and S. Seetharaman: *ISIJ Int*., 2002, vol. 42, pp. 155–62.
15. J.F. Xu, J.Y. Zhang, C. Jie, F. Ruan, and K.C. Chou: *Ironmak. Steelmak*., 2011, vol. 38, pp. 329–37.
16. W. Wang, K. Blazek, and A. Cramb: *Metall. Mater. Trans. B*, 2008, vol. 39B, pp. 66–74.
17. Z. Zhang, G. Wen, J. Liao, and S. Sridhar: *Steel Res. Int*., 2010, vol. 81, pp. 516–28.
18. H.G. Ryu, Z.T. Zhang, J.W. Cho, G.H. Wen, and S. Sridhar: *ISIJ Int*., 2010, vol. 50, pp. 1142–50.
19. L. Zhou, W. Wang, R. Liu, and B.G. Thomas: *Metall. Mater. Trans. B*, 2013, vol. 44B, pp. 1264–79.
20. L. Zhou, W. Wang, J. Wei, and M. Jin: *ISIJ Int*., 2013, vol. 53, pp. 671–74.
21. L. Zhou, W. Wang, F. Ma, J. Li, J. Wei, H. Matsuur, and F. Tsukihashi: *Metall. Mater. Trans. B*, 2012, vol. 43B, pp. 354–62.
22. M. Allibert, H. Gaye, J. Geiseler, D. Janke, B.J. Keene, D. Kirner, M. Kowalski, J. Lehmann, K.C. Mills, D. Neuschutz, R. Parra, C. Sanint-Jours, R.J. Spencer, M. Susa, M. Tmar, and E. Woermann: *Slag Atlas*, 2nd ed., Verlag Stahleisen GmbH, D-Dusseldorf, Germany, 1995.
23. Y. Kashiwaya, C.E. Cicutti, and A. Cramb: *ISIJ Int*., 1998, vol. 38, pp. 357–65.
24. N.X. Sun, X.D. Liu, and K. Lu: *Scripta Mater*., 1996, vol. 34, pp. 1201–07.
25. W. Wang: PhD Thesis, Carnegie Mellon University, 2007.
26. B. Nan: PhD Thesis, Carnegie Mellon University, 2007.
27. A.A. Elabbar, M. Abu El-Oyoun, and A.A. Abu-Sehly: *JTUSCI*, 2008, vol. 1, pp. 44–50.
28. J.H. Park, D.J. Minand, and H.S. Song: *Metall. Mater. Trans. B*, 2004, vol. 35B, pp. 269–75.
29. J.H. Heo, S.S. Park, and J.H. Park: *Metall. Mater. Trans. B*, 2012, vol. 43B, pp. 1098–1105.
30. G. Kim, C. Kim, and I.L. Sohn: *ISIJ Int*., 2013, vol. 53, pp. 170–76.
31. W. Christian: *The Theory of Transformations in Metals and Alloys*, 3rd ed., Pergamon Press Ltd, London, 2002.
32. J.K. Prapakorn: PhD Thesis, Carnegie Mellon University, 2003.
33. D.R. MacFarlane and M. Fragoulis: *Phys. Chem. Glasses*, 1986, vol. 37, pp. 228–34.